frontiers | Frontiers in Astronomy and Space Sciences

TYPE Original Research
PUBLISHED 21 October 2022
DOI 10.3389/fspas.2022.952486

Check for updates

OPEN ACCESS

EDITED BY
Joseph E. Borovsky,
Space Science Institute, United States

REVIEWED BY
Richard Boynton,
The University of Sheffield,
United Kingdom
Chongjing Yuan,
Institute of Geology and Geophysics (CAS), China

*CORRESPONDENCE
Sneha A. Gokani,
gokanisneha@gmail.com

SPECIALTY SECTION
This article was submitted to Space Physics, a section of the journal Frontiers in Astronomy and Space Sciences

RECEIVED 25 May 2022
ACCEPTED 07 October 2022
PUBLISHED 21 October 2022

CITATION
Gokani SA, Han D-S, Selvakumaran R and Pant TK (2022), Dependence of radiation belt flux depletions at geostationary orbit on different solar drivers during intense geomagnetic storms.
Front. Astron. Space Sci. 9:952486.
doi: 10.3389/fspas.2022.952486

COPYRIGHT
© 2022 Gokani, Han, Selvakumaran and Pant. This is an open-access article distributed under the terms of the Creative Commons Attribution License (CC BY). The use, distribution or reproduction in other forums is permitted, provided the original author(s) and the copyright owner(s) are credited and that the original publication in this journal is cited, in accordance with accepted academic practice. No use, distribution or reproduction is permitted which does not comply with these terms.

Dependence of radiation belt flux depletions at geostationary orbit on different solar drivers during intense geomagnetic storms

Sneha A. Gokani[1,2]*, De-Sheng Han[1], R. Selvakumaran[1,2] and Tarun Kumar Pant[2]

[1]State Key Laboratory of Marine Geology, School of Ocean and Earth Science, Tongji University, Shanghai, China, [2]Space Physics Laboratory, Vikram Sarabhai Space Centre, Thiruvananthapuram, India

The loss of electron flux of the outer radiation belt has been widely studied in terms of the mechanism that brings in these losses. There are a few studies which have attempted to explain the interplanetary conditions that favor the depletions. As the Sun is the prime cause of any change happening in the magnetosphere, it is important to look at the solar drivers that bring in such changes. In this study, we attempt to understand the effect of solar structures and substructures on the loss of radiation belt high-energy electrons during intense geomagnetic storms. The superposed epoch analysis is used to observe any peculiar changes in GOES electron flux data during the storms that are associated with solar structures such as CME and CIR, ICME substructures such as the magnetic cloud, magnetic cloud with sheath, ejecta, ejecta with sheath, and only sheath. The long-term data also give an opportunity to compare the flux decrease during solar cycles 23 and 24. It has been observed that 1) CIR-associated storms cause a comparatively higher flux decrease than CME-associated storms, 2) sheath-related storms bring out a higher flux decrease, and 3) there is no significant change in flux for the storms of both the solar cycles. The flux decrease in intense storms at the geostationary orbit is essentially triggered by the "Dst effect." Apart from this, the minimum IMF Bz and northward IMF Bz before turning southward add to the flux decrease. These results hold true for the electron depletions occurring only during intense geomagnetic storms and may alter otherwise.

KEYWORDS

radiation belt, solar wind, solar drivers, geomagnetic storms, electron flux depletion

Introduction

The outer radiation belts are very much vibrant in the sense that they undergo many dynamic processes such as particle acceleration (Summers et al., 1998; Friedel et al., 2002; Elkington et al., 2003; Meredith et al., 2003; Horne et al., 2005; Reeves et al., 2013), transport (Lyons & Thorne, 1973; Baker et al., 2007), and loss (Iles et al., 2002; Onsager

et al., 2002; Reeves et al., 2003; Bortnik et al., 2006; Millan & Thorne, 2007; Baker et al., 2016). Among these processes, the true loss of radiation belt particles is of prime concern because they can cause significant spacecraft operational anomalies (Baker et al., 1987; Allen, 2002; Baker et al., 2004), sometimes causing permanent damage to space systems (Baker et al., 2018) and posing a threat to the climate through instances of highly energetic electron precipitation into the atmosphere (Clilverd et al., 2016; Tsurutani et al., 2016; Baker et al., 2018). These reasons make it necessary to thoroughly study the outer belt particle losses, especially of the highly energetic electrons.

Many researchers have given special attention to understand the mechanism behind the true loss of these electrons. The observed loss of electron flux is attributed to adiabatic losses (McIlwain, 1966; Kim and Chan, 1997) or real losses either by magnetopause shadowing (Shprits et al., 2006; Baker et al., 2016; Herrera et al., 2016; Zhang et al., 2016) or precipitation into the atmosphere (Thorne & Kennel, 1971; Green et al., 2004; Turner et al., 2014; Shprits et al., 2016; Tsurutani et al., 2016; Pham et al., 2017) by resonant wave–particle interaction. Li et al. (1997) used multi-satellite observations during geomagnetic storms to suggest adiabatic losses in the inner part of the belt, whereas nonadiabatic losses in the outer part. Later, Onsager et al. (2002) also came to a similar conclusion by using multi-spacecraft observations. Bortnik et al. (2006) suggested that at high L-shells ($L > 5$), the dropout is independent of energy and caused due to magnetopause shadowing in addition to radial diffusion, whereas at $L < 5$, the dropout is strongly energy dependent and caused due to electromagnetic ion cyclotron (EMIC)–driven pitch angle scattering. Contradicting results have been obtained by Xiang et al. (2017), suggesting the importance of μ and K dependence of electron phase space density (PSD) in understanding the dropout mechanism.

Very few studies have focused on the influence of different interplanetary parameters on the loss of radiation belt electrons. Borovsky and Denton (2010) studied the solar wind effect on electron flux dropouts during geomagnetic storms, using superposed epoch analysis. Similar studies have been undertaken by Meredith et al. (2011) for high-speed solar wind (HSS)–driven storms and by Yuan and Zong (2013). They concluded that the southward interplanetary magnetic field (IMF) and high pressure led to the strongest dropouts. Gao et al. (2015) also came to a similar conclusion by studying the dropouts occurring during both storm and non-storm periods for >2 MeV electrons. Boynton et al. (2016, 2017) carried out an error reduction ratio analysis to explore the nonlinear relationship between electron dropouts and solar wind, as well as other geomagnetic indices. Ni et al. (2016) from their study of the dynamic response of the Earth's radiation belts during periods of solar wind dynamic pressure pulse based on normalized superposed epoch analysis suggested that deeper earthward magnetopause erosion provides favorable conditions for the prompt occurrence of dropout at lower L-shells ($L < 5$). Pinto et al. (2018) by using GOES 8 and 10 electron flux data of energy >2 Mev studied the role of interplanetary parameters on the relativistic flux enhancements and persistent depletion events. These studies have established the role of solar wind conditions in favoring the radiation belt electron losses. From their study on the interplanetary shock properties and preconditions, Yue and Zong (2011) concluded that the perpendicular shock can produce more intense geomagnetic disturbance under the same IMF precondition. They also suggested that the interplanetary shocks can intensify the southward IMF precondition by a factor of 3–6. This study suggests that the orientation of the shocks and preconditioning are also important while considering their impact on the magnetosphere. As the Sun is the ultimate source of any change seen in the interplanetary medium, it thereby causes the magnetosphere to alter. This fact highlights the importance of studying the effect of various solar drivers on the radiation belt electron flux decrease. There are very few studies which have attempted to understand the effect of different solar structures on the radiation belt electron fluxes. Benacquista et al. (2018) studied the impact of two different solar structures, that is, the corotating interaction region (CIR) and interplanetary coronal mass ejection (ICME), on the variations of radiation belt electron fluxes. Their study revealed that the ICMEs are effective at all L-shells, whereas the CIRs have much less access to the innermost parts of the belts. Recently, Turner et al. (2019) showed that storms driven by coronal mass ejection (CME) sheaths or CME ejecta only are capable of producing prolonged depletions of multi-MeV electrons throughout the outer belt. By contrast, storms driven by full CMEs and stream interaction regions are prone to enhance MeV electrons. All these studies suggest the complexity and diversity of the radiation belt response to a space weather event at a given point of time. There has been ample research on the loss mechanism of the outer belt energetic electrons and also on the solar wind conditions which favor these losses. But, there are very few studies which have established a link between the solar structures and outer radiation belt response. Different heliospheric structures interact with the magnetosphere differently through variable forcing (Kilpua et al., 2009). All these in turn affect the response of the radiation belt electron flux. Not only the conditions within these structures are important but also in a broader way, the impacts these structures have can be different. There are still few open questions that need to be answered: 1) how differently do solar structures affect the energetic electron population of the outer radiation belt? 2) Why do two similar solar structures have different impacts on the magnetosphere? 3) Can we anticipate the response of the radiation belt if we know a particular solar structure is heading towards the Earth? 4) Is there any variation in the radiation belt flux from one solar cycle to another? In the present study, we try to investigate the response of the energetic electrons in terms of flux depletion to different solar structures. The long-term data set also provides an opportunity

10.3389/fspas.2022.952486

TABLE 1 List of events considered in this study along with the GOES spacecraft, the energy channel used, and the type of solar structure associated.

Sr. No.	Date	Spacecraft	Energy channel	Type of solar structure
1	23 October 1996	GOES 8	>0.6 MeV	CIR
2	21 April 1997	GOES 8	>0.6 MeV	MC
3	15 May 1997	GOES 8	>0.6 MeV	MC
4	11 October 1997	GOES 8	>0.6 MeV	MC
5	07 November 1997	GOES 8	>0.6 MeV	EJ-S
6	23 November 1997	GOES 8	>0.6 MeV	MC
7	18 February 1998	GOES 8	>0.6 MeV	MC
8	10 March 1998	GOES 8	>0.6 MeV	CIR
9	04 May 1998	GOES 8	>0.6 MeV	S
10	26 June 1998	GOES 8	>0.6 MeV	EJ
11	06 August 1998	GOES 8	>0.6 MeV	EJ
12	27 August 1998	GOES 8	>0.6 MeV	EJ
13	25 September 1998	GOES 8	>0.6 MeV	EJ
14	19 October 1998	GOES 8	>0.6 MeV	MC
15	08 November 1998	GOES 8	>0.6 MeV	EJ
16	09 November 1998	GOES 8	>0.6 MeV	S
17	13 November 1998	GOES 8	>0.6 MeV	MC
18	13 January 1999	GOES 8	>0.6 MeV	MC
19	18 February 1999	GOES 8	>0.6 MeV	EJ
20	22 September 1999	GOES 8	>0.6 MeV	EJ
21	22 October 1999	GOES 8	>0.6 MeV	EJ-S
22	13 November 1999	GOES 8	>0.6 MeV	MC
23	12 February 2000	GOES 8	>0.6 MeV	S
24	07 April 2000	GOES 8	>0.6 MeV	EJ-S
25	24 May 2000	GOES 8	>0.6 MeV	EJ
26	16 July 2000	GOES 8	>0.6 MeV	MC-S
27	11 August 2000	GOES 8	>0.6 MeV	EJ
28	12 August 2000	GOES 8	>0.6 MeV	MC
29	17 September 2000	GOES 8	>0.6 MeV	MC-S
30	05 October 2000	GOES 8	>0.6 MeV	EJ
31	14 October 2000	GOES 8	>0.6 MeV	MC
32	29 October 2000	GOES 8	>0.6 MeV	MC
33	06 November 2000	GOES 8	>0.6 MeV	MC
34	29 November 2000	GOES 8	>0.6 MeV	EJ
35	20 March 2001	GOES 8	>0.6 MeV	MC
36	31 March 2001	GOES 8	>0.6 MeV	MC-S
37	11 April 2001	GOES 8	>0.6 MeV	EJ
38	18 April 2001	GOES 8	>0.6 MeV	MC
39	22 April 2001	GOES 8	>0.6 MeV	MC-S
40	17 August 2001	GOES 8	>0.6 MeV	EJ
41	26 September 2001	GOES 8	>0.6 MeV	EJ
42	01 October 2001	GOES 8	>0.6 MeV	MC
43	03 October 2001	GOES 8	>0.6 MeV	MC
44	21 October 2001	GOES 8	>0.6 MeV	EJ
45	28 October 2001	GOES 8	>0.6 MeV	EJ
46	06 November 2001	GOES 8	>0.6 MeV	EJ
47	24 November 2001	GOES 8	>0.6 MeV	MC-S

(Continued on following page)

10.3389/fspas.2022.952486

TABLE 1 (*Continued*) List of events considered in this study along with the GOES spacecraft, the energy channel used, and the type of solar structure associated.

Sr. No.	Date	Spacecraft	Energy channel	Type of solar structure
48	24 March 2002	GOES 8	>0.6 MeV	MC
49	20 April 2002	GOES 8	>0.6 MeV	MC
50	11 May 2002	GOES 8	>0.6 MeV	EJ
51	23 May 2002	GOES 8	>0.6 MeV	MC
52	02 August 2002	GOES 8	>0.6 MeV	MC
53	21 August 2002	GOES 8	>0.6 MeV	EJ
54	04 September 2002	GOES 8	>0.6 MeV	CIR
55	08 September 2002	GOES 8	>0.6 MeV	EJ
56	01 October 2002	GOES 8	>0.6 MeV	MC
57	04 October 2002	GOES 8	>0.6 MeV	EJ
58	07 October 2002	GOES 8	>0.6 MeV	CIR
59	14 October 2002	GOES 8	>0.6 MeV	CIR
60	21 November 2002	GOES 8	>0.6 MeV	CIR
61	30 May 2003	GOES 8	>0.6 MeV	EJ
62	18 June 2003	GOES 10	>0.6 MeV	S
63	12 July 2003	GOES 10	>0.6 MeV	CIR
64	18 August 2003	GOES 10	>0.6 MeV	MC
65	30 October 2003	GOES 10	>0.6 MeV	MC
66	30 October 2003	GOES 10	>0.6 MeV	MC
67	20 November 2003	GOES 10	>0.6 MeV	MC
68	22 January 2004	GOES 10	>0.6 MeV	EJ
69	04 April 2004	GOES 10	>0.6 MeV	MC
70	25 July 2004	GOES 10	>0.6 MeV	MC
71	27 July 2004	GOES 10	>0.6 MeV	EJ
72	30 August 2004	GOES 10	>0.6 MeV	MC
73	08 November 2004	GOES 10	>0.6 MeV	MC
74	18 January 2005	GOES 10	>0.6 MeV	EJ
75	15 May 2005	GOES 10	>0.6 MeV	MC
76	30 May 2005	GOES 10	>0.6 MeV	EJ
77	13 June 2005	GOES 10	>0.6 MeV	MC
78	24 August 2005	GOES 10	>0.6 MeV	S
79	31 August 2005	GOES 10	>0.6 MeV	CIR
80	11 September 2005	GOES 10	>0.6 MeV	EJ
81	15 December 2006	GOES 10	>0.6 MeV	MC
82	06 August 2011	GOES 15	>0.8 MeV	EJ
83	26 September 2011	GOES 15	>0.8 MeV	EJ-S
84	25 October 2011	GOES 15	>0.8 MeV	MC
85	09 March 2012	GOES 15	>0.8 MeV	MC
86	24 April 2012	GOES 15	>0.8 MeV	MC
87	15 July 2012	GOES 15	>0.8 MeV	EJ
88	01 October 2012	GOES 15	>0.8 MeV	MC-S
89	09 October 2012	GOES 15	>0.8 MeV	MC
90	14 November 2012	GOES 15	>0.8 MeV	MC
91	17 March 2013	GOES 15	>0.8 MeV	MC-S
92	01 June 2013	GOES 15	>0.8 MeV	MC-S
93	29 June 2013	GOES 15	>0.8 MeV	S

(Continued on following page)

TABLE 1 (*Continued*) List of events considered in this study along with the GOES spacecraft, the energy channel used, and the type of solar structure associated.

Sr. No.	Date	Spacecraft	Energy channel	Type of solar structure
94	19 February 2014	GOES 15	>0.8 MeV	EJ-S
95	17 March 2015	GOES 15	>0.8 MeV	MC-S
96	23 June 2015	GOES 15	>0.8 MeV	MC
97	07 October 2015	GOES 15	>0.8 MeV	CIR
98	20 December 2015	GOES 15	>0.8 MeV	MC
99	01 January 2016	GOES 15	>0.8 MeV	MC
100	13 October 2016	GOES 15	>0.8 MeV	MC
101	28 May 2017	GOES 15	>0.8 MeV	MC
102	08 September 2017	GOES 15	>0.8 MeV	MC
103	26 August 2018	GOES 15	>0.8 MeV	MC

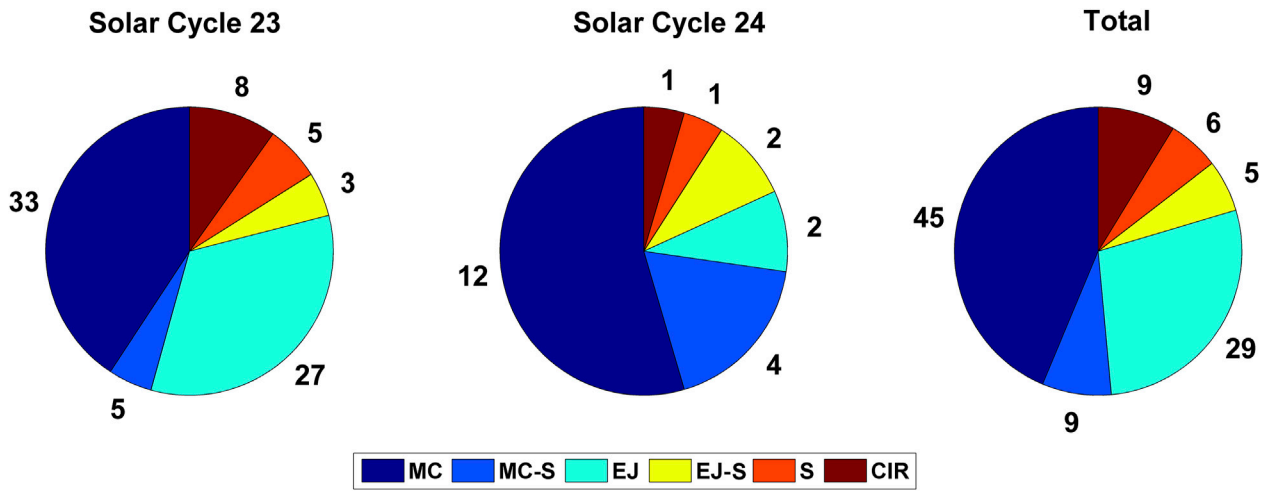

FIGURE 1
Number of storms that occurred due to different structures and substructures during solar cycles 23 and 24 (first and middle panels). A total of 103 storms are considered in this study, divided according to the solar drivers (last panel).

to compare this response over two solar cycles. We identified the flux depletions of electrons having energies >0.6 MeV and >0.8 MeV at the geostationary orbit during 103 intense geomagnetic storms that occurred between 1996 and 2019, which comprises solar cycles 23 and 24. We performed the epoch analysis to understand the contribution of different solar wind and interplanetary conditions. We have divided the events as per the solar structure which drives the changes in the magnetosphere. Firstly, the solar structures are characterized as CME or CIR. When it is CME, then depending on the ICME structure, they are further divided into magnetic cloud (MC), ejecta (EJ), sheath (S), magnetic cloud with sheath (MC-S), and ejecta with sheath (EJ-S).

Materials and methods

The intense geomagnetic storms (Dst ≤ −100 nT) that have occurred during solar cycles 23 and 24 were identified from the World Data Center (http://wdc.kugi.kyoto-u.ac.jp/dst_final/index.html). A total of 103 intense geomagnetic storms had been identified from 1996 to 2019. In order to check the electron depletions during all the selected events, the electron flux data of energy >0.6 MeV was obtained from the Geostationary Operational Environmental Satellite (GOES) 8 and 10 till 2006. From 2011 onward, we have made use of >0.8 MeV channel from GOES 15 spacecraft. The list of the energy channels and spacecraft used is given in Table 1.

These data can be found at https://www.ngdc.noaa.gov/stp/satellite/goes/dataaccess.html. We made use of the OMNIWeb data (https://omniweb.gsfc.nasa.gov/form/dx1.html) to identify solar structures and substructures. The same set of data was used to examine the interplanetary conditions during the flux depletion events. Figure 1 shows the number of geomagnetic storms that occurred during solar cycles 23 and 24, which are further divided into solar structures such as CME and CIR. A total of 81 intense geomagnetic storms occurred during solar cycle 23, out of which 73 were associated with CME and 8 were associated with CIR. As we all know, solar cycle 24 was mild. It consisted of only 22 intense geomagnetic storms, out of which 21 were associated with CME and only 1 was associated with CIR. The CMEs were further divided into ICME substructures such as MC, MC-S, EJ, EJ-S, and S.

The identification of CMEs that occurred in solar cycle 23 was done using the catalog by Gopalswamy et al. (2010) along with the list provided by Richardson and Cane (2010). The identification of CMEs that occurred in solar cycle 24 was done by running movies of coronagraph images available at https://cdaweb.gsfc.nasa.gov. Few of the CMEs were identified using the list provided by Richardson and Cane (2010). The storms which were not associated with CME were checked for any CIR association. Such storms were identified using WIND and ACE observations. Furthermore, the substructures of CMEs were identified by their signatures in interplanetary data. The magnetic clouds (MC) were thought to have one or more of the following signatures: 1) strong magnetic field, 2) smooth latitudinal rotation of the field, and 3) low proton temperature or plasma β (Selvakumaran et al., 2016). Whereas, ejecta (EJ) had 1) a comparatively weaker magnetic field, 2) higher proton temperature or higher plasma β, 3) no clear rotation in the magnetic field, and 4) an enhanced N_α/Np ratio (Gopalswamy et al., 2010). During sheaths, no particular change was observed in plasma β, and there was no smooth rotation of the magnetic field. Major events were taken from the MC list provided by Gopalswamy et al. (2015). Other events were identified by ourselves. The respective number of storms in each category is presented in Figure 1. The storms that occurred due to MC are dominant in both solar cycles, making 45 out of a total of 103 storms, followed by 29, 9, 6, and 5 storms associated with EJ, MC-S, S, and EJ-S, respectively.

Epoch analysis was carried out to understand the effect of different solar drivers on the relativistic electron flux decrease at a geostationary orbit. The time of minimum Dst was taken as the epoch. The flux decrease (ΔF) was calculated by subtracting the minimum flux from the pre-depletion value. To do this, the flux was normalized by the pre-depleted flux value. For easy understanding, we present these values in terms of the order of magnitude. We took care of the flux depletions that occurred on the same day but not during the storm period, that is, we strictly chose the depletions that occurred during the main phase of the geomagnetic storm.

Observations and results

A total of 103 intense geomagnetic storms were considered in this study that had occurred from 1996 to 2019, comprising two solar cycles. The reason behind choosing only intense storms is that not all storms produce electron flux depletions (Reeves et al., 2003). The main motive of this study was to check the dependence of electron flux decrease on different solar drivers. We calculated the level of flux decrease for each of the storms after performing superposed epoch analysis and tried to find any relationship that it may have with different solar drivers.

Epoch analysis

With the time of minimum Dst as an epoch, the epoch analysis was performed on various interplanetary conditions for different solar drivers. The magnetopause standoff distance was also considered in the analysis, which was calculated by using the model given by Shue et al. (1997). We chose a time window of 1 day before and after the epoch to examine full depletion till its recovery. Figure 2 represents the mean value of A) IMF Bz (nT); B) solar wind speed, Vsw (km/h); C) solar wind density, Np (n/cc); D) solar wind dynamic pressure, Pdy (nPa); E) electric field (V/m); F) Sym-H (nT); G) magnetopause stand-off distance, R_0 (R_E); and H) GOES >0.6 MeV electron flux (e cm^{-2} s^{-1} sr^{-1}) for the different abovementioned ICME structures, shown using different colors. From the figure, it can be seen that the level of electron flux decrease is independent of the Sym-H values. This analysis reveals that the storms which are associated with sheath (MC-S, EJ-S, and S) show more flux decrease (ΔF) than non-sheath drivers (MC and EJ). The highest flux decrease (in the order of magnitude) of ~3.0 ± 0.6 was seen for the storms associated with sheath, followed by ~2.7 ± 0.6 for EJ-S, ~2.4 ± 0.55 for MC-S, ~1.9 ± 0.4 for MC, and ~1.6 ± 0.35 for EJ. At none of the times was the magnetopause pushed beyond 6.2 R_E.

Figures 3A–H are in a similar format as Figures 2A–H, but for solar structures such as CME and CIR. From the figure, it can be seen that the flux decrease is more, with $\Delta F \approx 2.2 \pm 0.35$ order of magnitude for the storms that are associated with CIR. The storms associated with CME show comparatively lesser flux decrease with $\Delta F \approx 1.7 \pm 0.41$ order of magnitude, even though the Sym-H is high for CME-related storms.

A similar analysis was carried out for the storms that occurred during solar cycles 23 and 24, as shown in Figures 4A–H. It is in the same format as Figures 2, 3. Though the number of intense storms had decreased drastically, almost by ~57% in solar cycle 24 when compared to solar cycle 23, no difference is seen in the level of electron flux decrease (Figure 4H). It is ~1.69 ± 0.35 for solar cycle 23 and ~1.77 ± 0.4 for solar cycle 24. However, it can be noticed that the overall flux level is significantly lower for the storms that occurred in solar cycle 24 than for those that occurred in solar cycle 23.

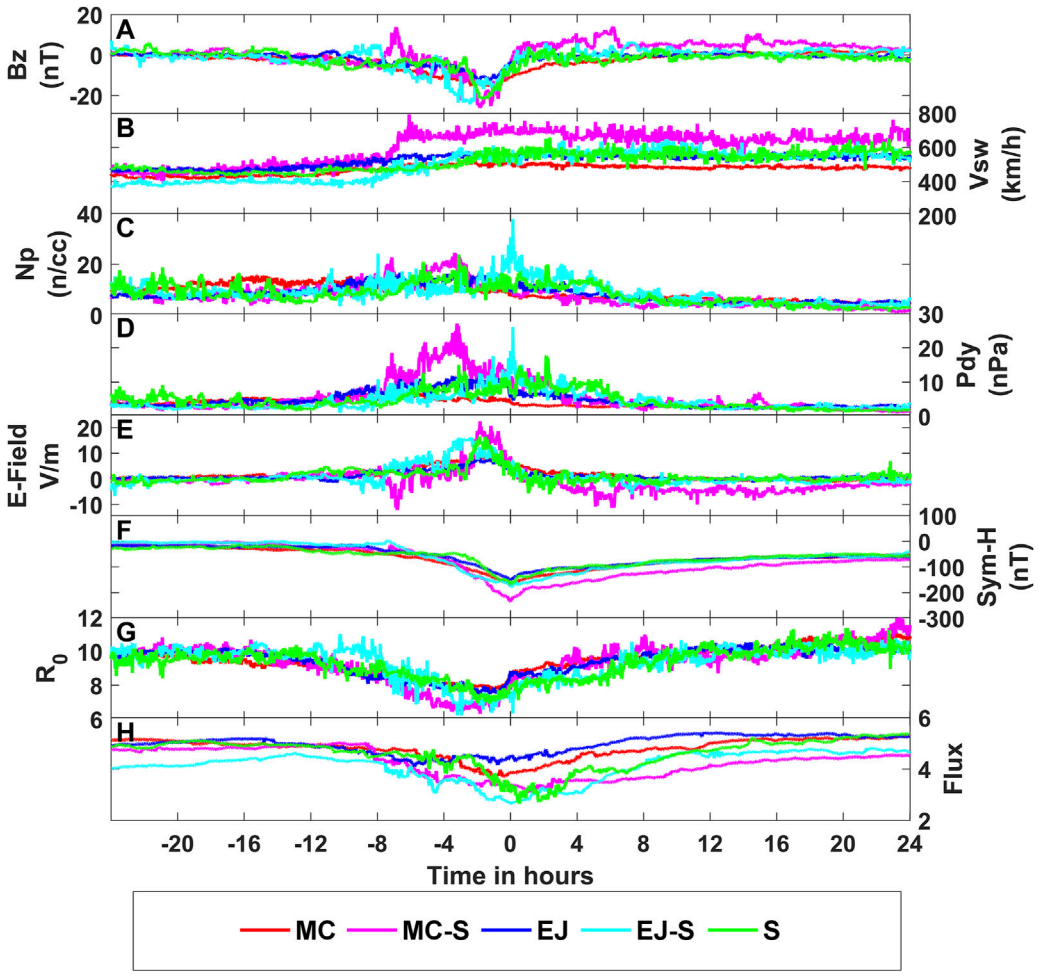

FIGURE 2
Superposed epoch analysis performed on the various interplanetary conditions: **(A)** IMF Bz (nT), **(B)** solar wind speed, Vsw (km/h), **(C)** solar wind density, Np (n/cc), **(D)** solar wind dynamic pressure, Pdy (nPa), **(E)** electric field (V/m), **(F)** Sym-H (nT), **(G)** magnetopause stand-off distance, R_0 (R_E), and **(H)** GOES >0.6 MeV electron flux (e cm^{-2} s^{-1} sr^{-1}) for different solar substructures such as magnetic cloud (MC), magnetic cloud with sheath (MC-S), ejecta (EJ), ejecta with sheath (EJ-S), and sheath (S) represented by different colors.

Effect of solar wind parameters

Some differences in maximum values of interplanetary conditions such as solar wind speed, pressure, density, and electric field are seen for different solar structures and substructures after performing epoch analysis, as seen in Figures 2, 3, respectively. Some previous studies had also examined the role of IMF Bz and solar wind dynamic pressure on radiation belt electron flux (Borovsky and Denton, 2010; Meredith et al., 2011; Yuan and Zong, 2013; Gao et al., 2015). Boynton et al. (2016)had carried out an error reduction ratio analysis and concluded that the solar wind dynamic pressure coupled with solar wind density are the main driving factors for the loss of electrons at energies 128 ≤ E ≤ 925 keV and the solar wind dynamic pressure coupled with southward IMF at energies 1.3 ≤ E ≤ 2 MeV at the geostationary orbits. We also tried to look at the role of solar wind dynamic pressure, speed, density, and electric field on flux depletions. The effect of IMF Bz is studied separately in the next section. We used maximum values of solar wind dynamic pressure, speed, density, and electric field obtained after epoch analysis to check its influence on the level of flux decrease described in terms of the order of magnitude, as shown in Figure 5 for different solar structures and substructures. Seen superimposed on it is an IMF Bz, which is divided into two groups, *viz.*, IMF Bz < −20 nT (big circles) and IMF Bz > −20 nT (small circles). From the figure, it is evident that most of the flux depletion is accompanied by strong southward IMF Bz. All the CIR-related storms are produced by IMF Bz > −20 nT. It

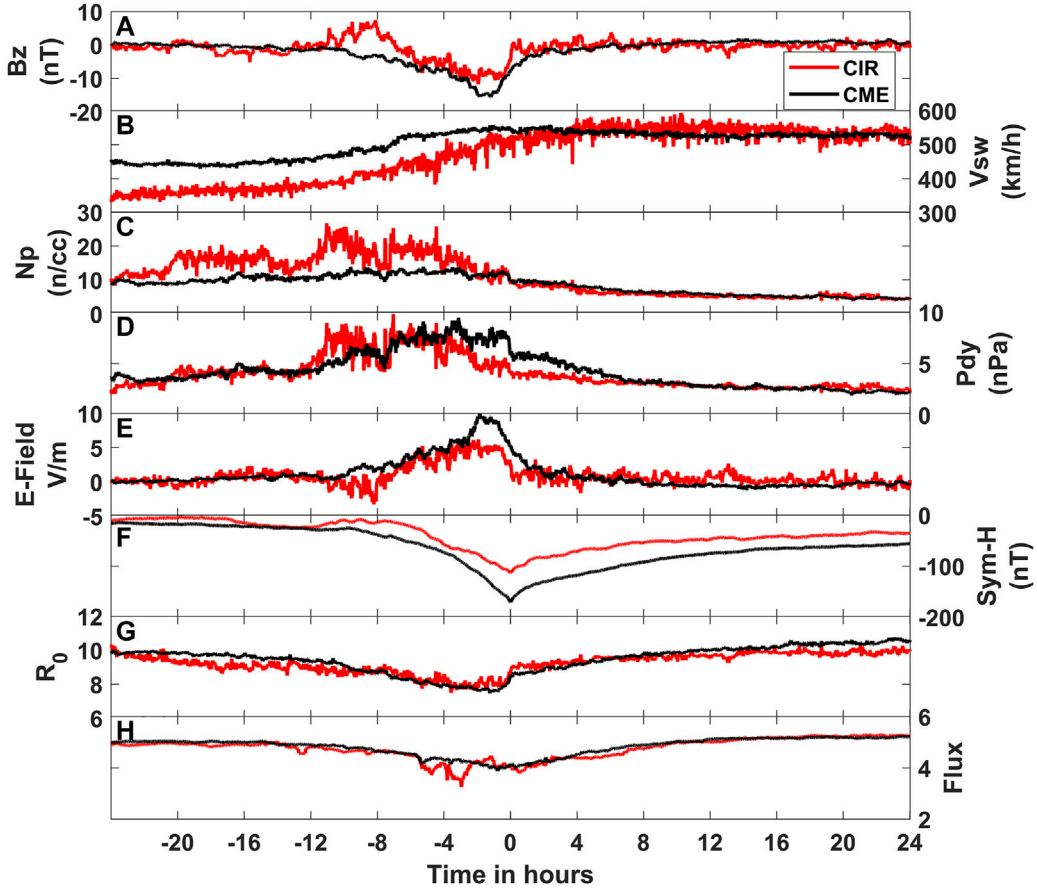

FIGURE 3
Superposed epoch analysis performed on the various interplanetary conditions: **(A)** IMF Bz (nT), **(B)** solar wind speed, Vsw (km/h), **(C)** solar wind density, Np (n/cc), **(D)** solar wind dynamic pressure, Pdy (nPa), **(E)** electric field (V/m), **(F)** Sym-H (nT), **(G)** magnetopause stand-off distance, R_0 (R_E), and **(H)** GOES >0.6 MeV electron flux (e cm^{-2} s^{-1} sr^{-1}) for different solar structures such as CME (black curve) and CIR (red curve).

can also be seen that there is no significant difference in the values of Vmax, Nmax, Pmax, and Emax for the storms associated with different solar drivers. The average values of Vmax, Nmax, Pmax, and Emax along with flux decrease (ΔF) for different solar drivers are given in Table 2. Figure 6 is similar to Figure 5, with R_0 superimposed instead of IMF Bz. Here, R_0 is categorized in two groups, *viz.*, $R_0 < 6$ (small circles) and $R_0 \geq 6$ (big circles). From the figure, it can be seen that in most of the cases, the magnetopause did not move inward beyond the geostationary orbit. This suggests that essentially, the flux decrease is governed by the 'Dst effect' (McIlwain, 1966). Having said that, one cannot neglect the effects of wave–particle interactions during such events. Table 3 shows the number of events for $R_0 < 6$ R_E and $R_0 \geq 6$ R_E. It can be seen that during the storms that are associated with sheaths (MC-S, EJ-S, and S), mostly the magnetopause is pushed inward with $R_0 < 6$. During such cases, the magnetopause shadowing effect may dominate. The sheath passages also favor ULF waves to grow and therefore deplete the particles under the influence of pitch angle scattering.

Dependence of IMF Bz

Apart from solar wind parameters, IMF Bz has been observed to show peculiar features during electron flux depletions. Gao et al. (2015) have shown that the strong southward IMF Bz is solely capable of significant relativistic electron depletions. Figure 2 shows that in some cases, IMF Bz is seen to turn northward before turning southward during the course of flux decrease. To check the effect in detail, we plotted ΔF against IMF Bz for A) MC, B) MC-S, C) EJ, D) EJ-S, and E) S, as shown in Figure 7. The IMF Bz and flux values are of 1 min resolution and are mean values taken after performing epoch analysis during the course of flux depletion. From the figure, it can be noted that the storms that are associated with MC-S, EJ-S, and S show more positive IMF Bz values (fourth quadrant), for which the flux

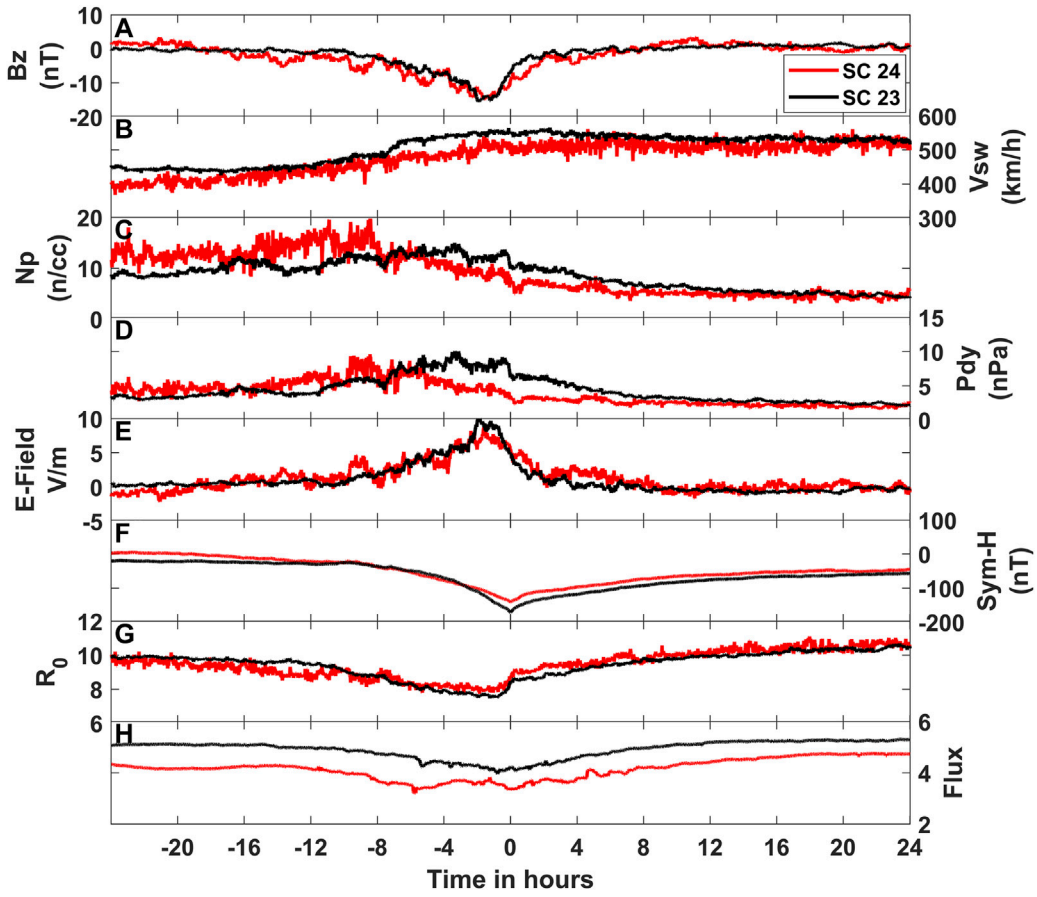

FIGURE 4
Superposed epoch analysis performed on the various interplanetary conditions: **(A)** IMF Bz (nT), **(B)** solar wind speed, Vsw (km/h), **(C)** solar wind density, Np (n/cc), **(D)** solar wind dynamic pressure, Pdy (nPa), **(E)** electric field (V/m), **(F)** Sym-H (nT), **(G)** magnetopause stand-off distance, R_0 (R_E), and **(H)** GOES >0.6 MeV electron flux (e cm^{-2} s^{-1} sr^{-1}) for the storms those occurred during solar cycle 23 (black curve) and solar cycle 24 (red curve).

decrease is seen to be comparatively high. Also, we can see that the storms associated with these drivers have a minimum Bz exceeding −20 nT, whereas the storms associated with the other two categories have a minimum Bz < −15 nT. A similar trend is observed for storms triggered by CIR when compared to CME, as shown in Figure 8. Here also, the fourth quadrant for CIR-related storms is dominant, highlighting the importance of northward IMF Bz before turning southward. A similar analysis is carried out for the storms of both solar cycles (Figure 9). However, no difference is seen either for positive IMF Bz values or minimum IMF Bz between the two, which may have led to no significant change in the level of flux decrease.

Discussion

By performing epoch analysis on the interplanetary conditions and GOES electron flux data, we tried to examine the effect of different solar drivers on the loss of radiation belt electron flux at geostationary orbit during intense geomagnetic storms. Reeves et al. (2003) analyzed the response of relativistic electrons to 276 moderate and intense (Dst < −50 nT) geomagnetic storms. They observed that 56% of the storms showed an overall increase in the trapped flux, only 19% exhibited a decrease, while there was no flux change during 28% of the storms. This suggests the complexity in the response of relativistic electron flux to geomagnetic storms, and it is a delicate balance between acceleration and loss of the particles. As our focus was to analyze only the flux depletion and its dependence on various solar drivers, we chose the days of intense geomagnetic storms, which guaranteed only flux decrease. A total of 103 intense (Dst ≤ −100 nT) geomagnetic storms occurred during 1996–2019, which are considered in the present study, and the change in relativistic electron flux for E > 0.6 and > 0.8 MeV at geostationary orbit is observed using GOES electron flux measurements. A decrease of more than one order

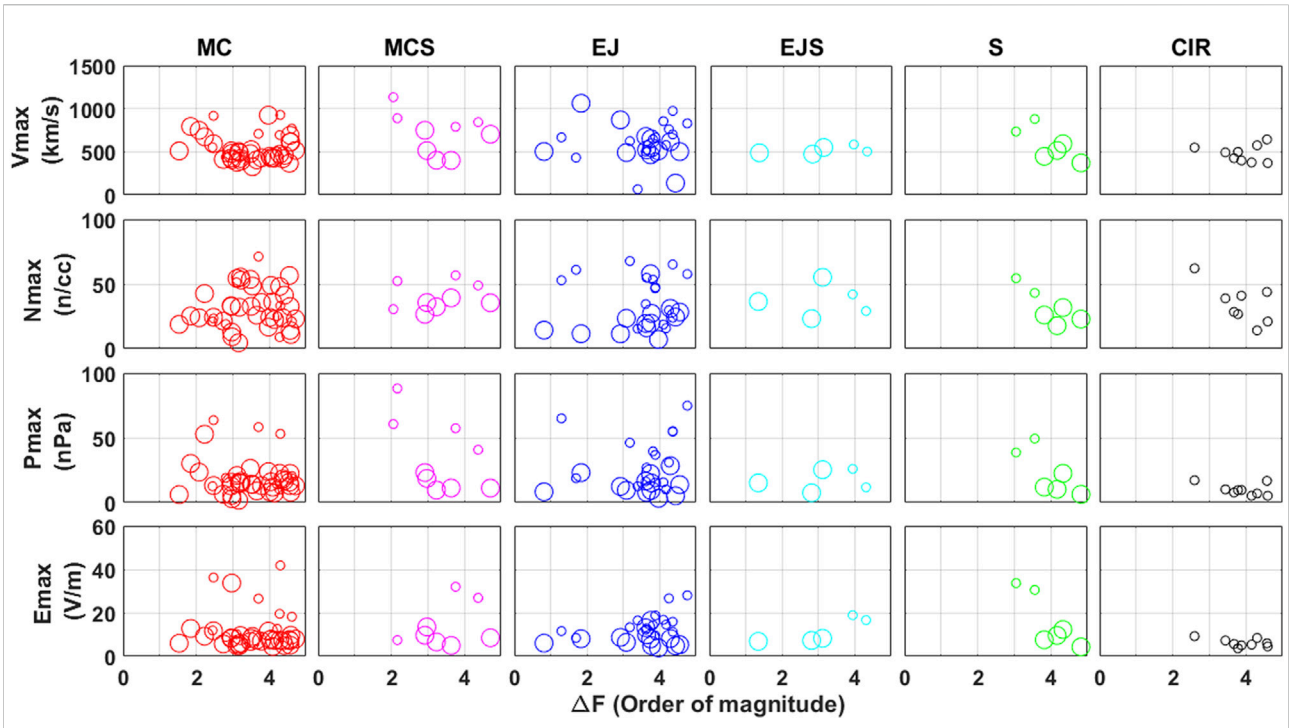

FIGURE 5
Variation of decrease in the electron flux (ΔF in orders of magnitude) with maximum solar wind speed (Vmax in km/s), density (Nmax in n/cc), pressure (Pmax in nPa), and electric field (Emax in V/m) for different solar drivers. Superimposed on that is the IMF Bz in two groups: IMF Bz > −20 nT (small circles) and IMF Bz < −20 nT (big circles).

TABLE 2 Average values of maximum solar wind speed (Vmax in km/s), density (Nmax in n/cc), dynamic pressure (Pmax in nPa), electric field (Emax in V/m), and electron flux decrease (ΔF in the order of magnitude) for different solar drivers after performing epoch analysis.

Type	Vmax (Km/s)	Nmax (n/cc)	Pmax (nPa)	Emax (V/m)	ΔF (ord. of mag.)
MC	521.7	15.53	7.306	9.113	1.2727
MC-S	793.6	24.46	27.1	22.48	1.8726
EJ	577.2	16.62	11.67	7.996	1.0932
EJ-S	640.4	37.82	26.09	15.97	1.5395
S	656.5	23.8	17.71	16.56	2.2656
CIR	593.7	26.67	9.818	6.19	1.5901

of magnitude is seen in the electron flux for all the events. The flux decrease is observed to start with the main phase of the geomagnetic storm. Many different mechanisms, right from the adiabatic process ("Dst effect"), magnetopause shadowing, and scattering of electrons into the loss cone by resonant wave–particle interaction, either alone or in combination act on these particles. There are numerous studies to find the exact mechanism behind electron flux depletion (Bortnik et al., 2006; Shprits et al., 2006; Kim et al., 2010; Turner et al., 2012; Turner et al., 2014; Yuan and Zong, 2013; Baker et al., 2016; Tsurutani et al., 2016; and references given in Millan and Thorne, 2007); however, very few studies have focused on the solar drivers and interplanetary conditions on facilitating electron depletions. In this study, we exclusively focus on the role of different solar structures, such as CME and CIR, and different substructures, such as magnetic cloud, magnetic cloud with sheath, ejecta, ejecta with sheath, and only sheath, in favoring the depletions. The space weather depends mainly on the condition of the Sun and its emissions that hit the Earth, thereby making it necessary to analyze any effect/process happening in the magnetosphere due to changes in solar drivers. As the radiation belt electron flux response is different for shocks, sheaths, and MCs, it is necessary to understand their short- and long-term effects along with their occurrence (Kilpua E. et al., 2017). We make use of superposed

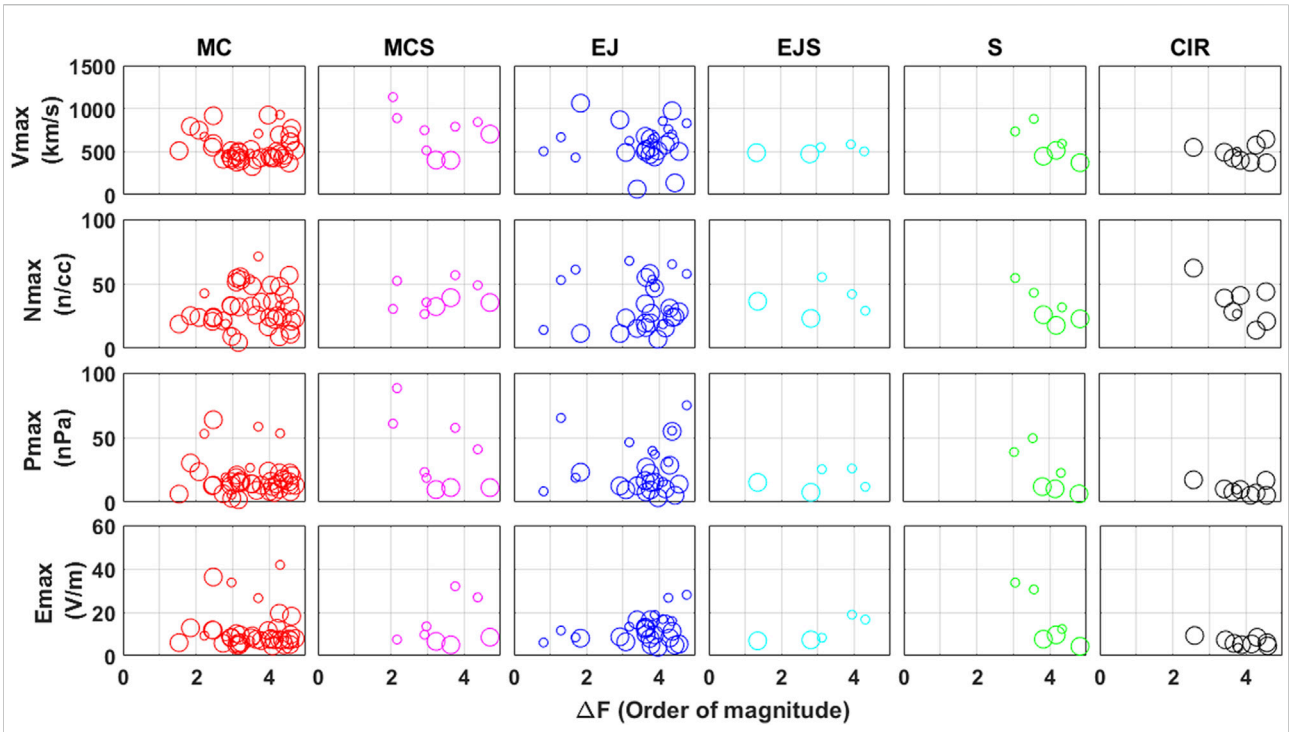

FIGURE 6
Variation of decrease in the electron flux (ΔF in orders of magnitude) with maximum solar wind speed (Vmax in km/s), density (Nmax in n/cc), pressure (Pmax in nPa), and electric field (Emax in V/m) for different solar drivers. Superimposed on that is the R_0 in two groups, $R_0 < 6\ R_E$ (small circles) and $R_0 \geq 6\ R_E$ (big circles).

TABLE 3 Number of events with $R_0 < 6$ and $R_0 \geq 6$ for different solar drivers.

Type	$R_0 < 6$	$R_0 \geq 6$	Total
MC	6	39	45
MC-S	6	3	9
EJ	10	19	29
EJ-S	3	2	5
S	3	3	6
CIR	1	8	9

epoch analysis to see the effect of the aforementioned solar drivers on the radiation belt electron loss. Gopalswamy et al. (2010) found that the CMEs with magnetic cloud (MC) structure are more geoeffective than the ejecta (EJ). We also found a higher degree of flux depletion for MC-related storms than for those related to EJ. We observed (from Figure 2) more flux depletion in the case of storms that are related to sheaths (MC-S, EJ-S, and S) than for the ones which are not (MC and EJ). Yermolaev et al. (2010) found that the geoeffectiveness of MC with sheath was the highest at 61%, that for EJ with sheath was 21%, and for the one without sheath had the lowest geoeffectiveness—only about 8%. The remaining contribution comes from only sheath and CIR-related storms. The sheath properties, which include high dynamic pressure (Palmroth et al., 2007; Myllys et al., 2016), enhanced ULF wave power in turn enhancing the viscous interactions at the magnetosphere (Borovsky and Funsten, 2003), and also stronger compression of the plasma and field caused by high Alfven Mach numbers (Borovsky and Brin, 2014; Myllys et al., 2016) all positively contribute toward the solar wind–magnetosphere coupling (Klipua et al., 2017b). However, the total energy input into the magnetosphere is larger during ICMEs without sheath due to their long encounters. The strong depleting tendency of the sheath-associated storms are presented in Figure 2 that may come from the pitch angle scattering and radial diffusion in combination with the highly compressed dayside magnetopause, due to enhanced ULF power and high dynamic pressure.

Though the storms associated with CME have been observed to be more geoeffective than the storms associated with CIR, we found that the radiation belt electron depletion is more in the latter case (Figure 3). Turner et al. (2019) observed enhancements of MeV electrons at higher L-shells ($L > 4.5$) after the initial depletion during the main phase of the storm. They also observed higher flux depletions for CME-related storms. However, our results

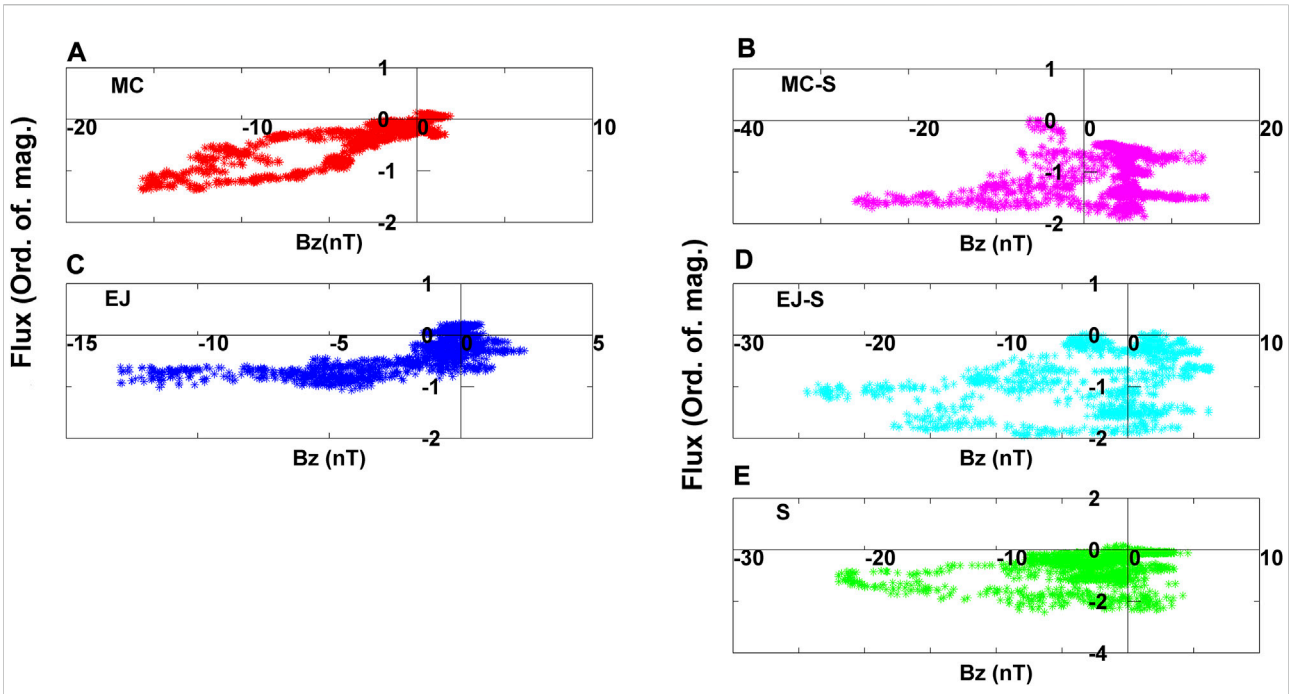

FIGURE 7
Variation of ΔF (in the order of magnitude) with IMF Bz (nT) for storms associated with **(A)** MC, **(B)** MC-S, **(C)** EJ, **(D)** EJ-S, and **(E)** S.

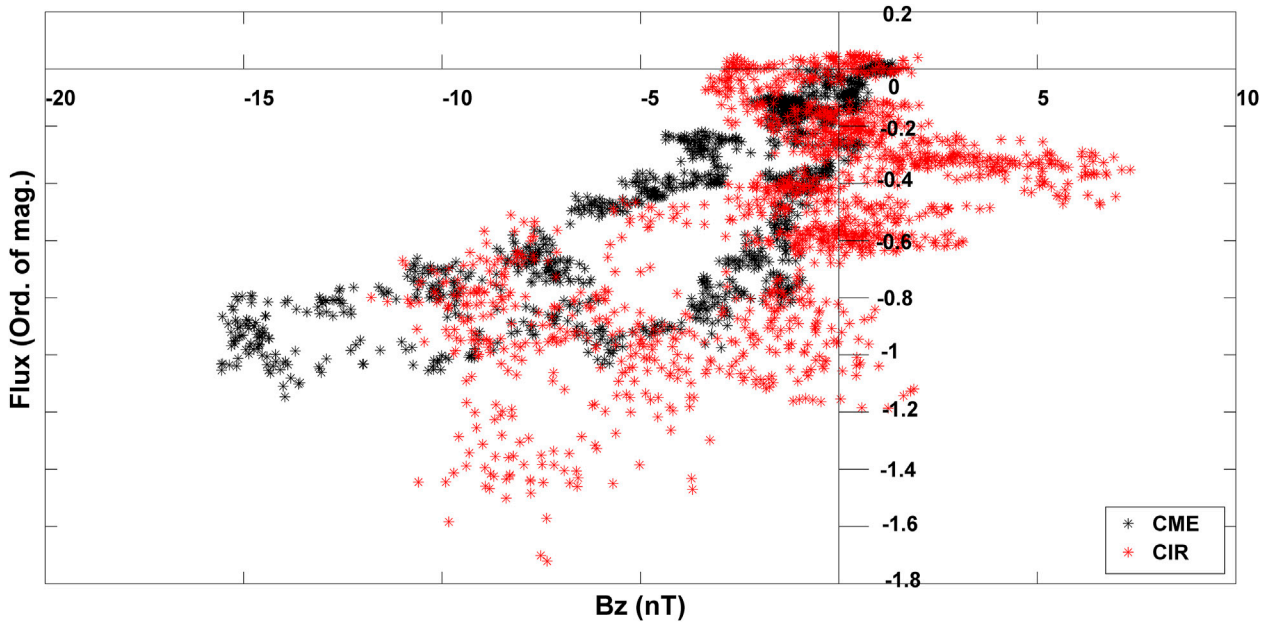

FIGURE 8
Variation of ΔF (in the order of magnitude) with IMF Bz (nT) for storms associated with CME (black) and CIR (red).

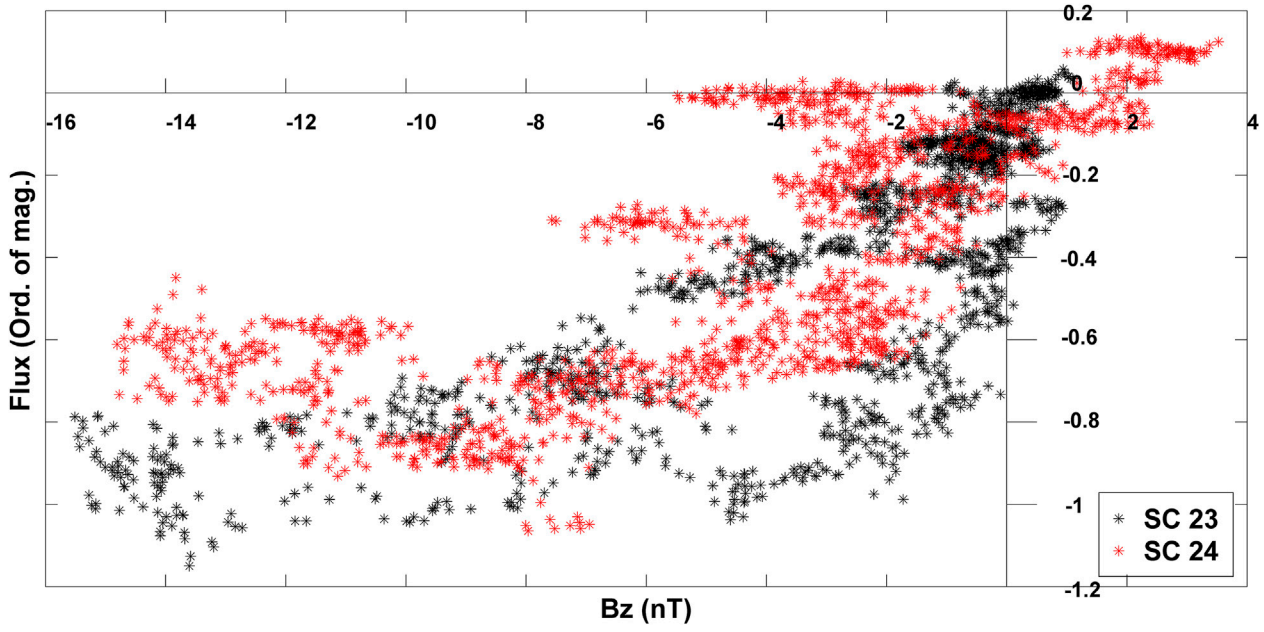

FIGURE 9
Variation of ΔF (in the order of magnitude) with IMF Bz (nT) for storms that occurred during solar cycle 23 (black) and solar cycle 24 (red).

contradict both these observations. We see a comparatively higher flux decrease for CIR-related storms. Also, we do not observe any flux enhancements after the initial depletion. Miyoshi and Kataoka (2005), after applying the superposed epoch analysis, also found that the CIRs tend to cause a much higher increase in the flux than ICMEs at the geosynchronous orbits. Benacquista et al. (2018) also supported the idea of flux increase on a large range of L* and decrease by only a limited number of CIR storms. Koskinen and Kilpua (2022) supported the idea of relativistic flux decrease during SIRs. The observations shown here are strictly during intense geomagnetic storms. Our results urge a reinvestigation of the comparison of flux decrease during CME- and CIR-driven intense geomagnetic storms.

We did not find any significant change in the level of flux decrease for the storms that occurred during the two solar cycles 23 and 24 (Figure 4), although the occurrence of intense geomagnetic storms had drastically decreased in solar cycle 24 (Figure 1). Selvakumaran et al. (2016) from their study on the comparison of moderate geomagnetic storms during solar cycles 23 and 24 observed a reduced magnetospheric energy transfer during solar cycle 24. Gopalswamy et al. (2015) from their study on the properties and geoeffectiveness of magnetic clouds during solar cycles 23 and 24 concluded that the geoeffectiveness was comparatively reduced during solar cycle 24 because of the anomalous CME expansion through its course in the interplanetary medium. Our results from Figure 4 show that the reduced geoefficiency or reduced magnetospheric energy transfer in solar cycle 24 has very less or no impact on the dynamics of radiation belt electron flux depletions.

The interplanetary and solar wind conditions also play an important role in causing radiation belt energetic electron flux decrease. We tried to understand the variations in the degree of flux decrease with different interplanetary properties such as solar wind pressure, speed, density, and electric field as shown in Figure 5 (which includes IMF Bz) and Figure 6 (which includes magnetopause distance). The high flux decrease is seen for the events when IMF Bz is < −20 nT. In most of the cases, the magnetopause did not cross the geostationary orbit, eliminating the possibility of magnetopause shadowing. For CIR-related storms, the influence of IMF Bz being comparatively less and $R_0 \geq 6$ suggest the importance of wave–particle interaction-driven pitch angle scattering as a cause for the flux decrease. As mentioned earlier, here the magnetopause distance is calculated using Shue et al. (1997) model. This model is widely and effectively used by many researchers like Turner et al. (2012), Gao et al. (2015), and Herrera et al. (2016). But, it should be kept in mind that the model values can have uncertainties and can vary from the actual values. Recently, Staples et al. (2020) constructed a database of ~20,000 spacecraft crossings of the dayside magnetopause and concluded that when the magnetopause is compressed below 8 R_E, the average measured location is >1 R_E inside the magnetopause. They also suggested that even extreme magnetopause events rarely reach the outer radiation belt. Our result that the magnetopause does not move beyond the geostationary orbit (~6 R_E) is in-line with the conclusions drawn by Staples et al. (2020). The solar wind pressure and speed seem to have an almost similar effect on the flux decrease.

Previous studies have only focused on the role of solar wind dynamic pressure, IMF Bz, and, up to some extent, solar wind speed. From their study on the correlation between relativistic electrons at GEO and properties of solar wind drivers during the solar minimum period, Blake et al. (1997) found that solar wind speed and density increase along with the southward turning of IMF leading to the enhancement of relativistic electrons. Many other studies have also found a positive correlation between the relativistic flux and solar wind speed (Baker et al., 1979; Paulika and Blake, 1979). Li et al. (2001) found solar wind speed to be the most important factor in their prediction model of electron fluxes at geostationary orbits. Some other studies have favored the role of high solar wind dynamic pressure and southward IMF Bz in reducing the relativistic electrons in the outer radiation belt (Borovsky and Denton, 2010; Meredith et al., 2011; Yuan and Zong, 2013; Gao et al., 2015).

The role of IMF Bz in the depletion of electron flux is analyzed separately as can be seen from Figures 7, 8, 9. We found two distinct features: 1) the flux decrease is more when there are more positive IMF Bz values and 2) the flux decrease is also more when the minimum negative Bz value is comparatively lesser. These two features are true for the cases of MC-S, EJ-S, S (Figures 7B,D,E), and CIR (Figure 8). Both of the features are absent in the case of comparison between solar cycles 23 and 24 where we do not observe much difference between the level of the flux. Gao et al. (2015), by analyzing the electron flux dropout events during storm and non-storm periods, found that when IMF Bz was southward, both the flux of precipitating electrons and the ratio between the precipitating electrons and trapped electrons were much larger. Our results show that the northward turning of IMF Bz before southward contributes positively toward more flux decrease. This can be visualized in the following way: during the course of positive Bz, the magnetosphere gets compressed and triggers the diffusion of the electrons to higher L-shells. Once the Bz turns southward, the magnetopause becomes eroded significantly due to enhanced magnetic reconnection. Souza et al. (2017) have studied the recovery of the relativistic radiation belt electrons and argue that the whistler mode chorus wave power is enhanced when IMF Bz is negative, on average, which in addition to amplification of magnetic integrated power in the ULF range accelerates the outer radiation belt electrons. Our study deals with the depletion of the electrons and suggests that the flux decrease is strengthened when IMF Bz turns southward after a significant positive course. Gao et al. (2015) suggested that the more stretched magnetic field during large solar wind dynamic pressure or southward IMF Bz intensifies the ring current. Then, the relativistic electrons are scattered as a result of deviation of the first adiabatic invariant. Our study not only stresses the importance of southward IMF Bz but also gives insight into the northward turning of IMF Bz before turning southward during a geomagnetic storm. We also suggest that the lesser negative Bz minimum leads to more flux decrease which can be attributed to maximum energy transfer during lesser southward IMF Bz (Selvakumaran et al., 2016).

By studying the depleting effects of ICME-driven sheath regions on the outer electron radiation belt, Hietela et al. (2014) suggested that under magnetospheric compression, the sheaths increase the radial diffusion that enhances the chances of magnetopause shadowing effects producing higher flux decrease. It is also believed that the fluctuating IMF Bz can launch magnetosonic waves, which propagate into the magnetosphere and can scatter the electrons into the loss cone by virtue of the resonant wave–particle interaction. Kilpua E. et al. (2017) has also claimed the dominating tendency of sheath passages in depleting the electrons. The results presented in this study suggest the importance of considering solar driver properties while anticipating the electron flux changes in the radiation belts. The detailed analysis of electron flux decrease at different L-shells using long-term data will be pursued in the future to add to the knowledge gained.

Summary and conclusion

A superposed epoch analysis is performed to investigate the effect of different solar structures and substructures on the depletion of relativistic electron flux at the geostationary orbit during the cases of intense geomagnetic storms. Our analysis found some interesting results:

1) Sheath-related storms (MC-S, EJ-S, and S) produce more flux decrease than the non-sheath ones (MC and EJ).
2) The increase in the solar wind pressure and speed increases the flux decrease.
3) Either northward IMF Bz before turning southward or rapidly fluctuating IMF Bz causes a higher flux decrease.

As the main aim of space weather studies is to know what, when, and how it will happen, our results presented here may provide a positive input to radiation belt modeling studies, while predicting the dynamics under particular solar and solar wind conditions.

Data availability statement

Publicly available data sets were analyzed in this study. These data can be found at OMNIWeb (https://omniweb.gsfc.nasa.gov/form/dx1.html), World Data Center, Kyoto (https://wdc.kugi.kyoto-u.ac.jp/dst_final/index.html), GOES (https://www.ngdc.noaa.gov/stp/satellite/goes/dataaccess.html), and CDAWeb (https://cdaweb.gsfc.nasa.gov).

Author contributions

SG, the first author has conceptualized the idea, carried out the analysis, written the manuscript, and contributed towards the physical interpretation of the results. DH has contributed towards interpreting the results and also provided the basic infrastructure to carry out the research. RS has identified the solar structures and substructures and

contributed in interpreting the results. TP has contributed towards interpreting the results.

Funding

This work is partly supported by the National Natural Science Foundation of China (42050410313, 42030101, and 41974185). SG carried out this work using the research grant from the Science and Engineering Research Board, Department of Science and Technology, India (2020/RJF/000125). RS acknowledges the support from the research grant from the Science and Engineering Research Board, Department of Science and Technology, India (PDF/2021/002226).

Acknowledgments

The authors thank the head of the School of Ocean and Earth Sciences for supporting the research work. They also thank SPL and VSSC for encouraging the research activities toward this work and the OMNIWeb (https://omniweb.gsfc.nasa.gov/form/dx1.html) team for providing solar wind data. They also thank the World Data Center, Kyoto, for providing Dst values (https://wdc.kugi.kyoto-u.ac.jp/dst_final/index.html), GOES (https://www.ngdc.noaa.gov/stp/satellite/goes/dataaccess.html) team, and CDAWeb (https://cdaweb.gsfc.nasa.gov).

Conflict of interest

The authors declare that the research was conducted in the absence of any commercial or financial relationships that could be construed as a potential conflict of interest.

Publisher's note

All claims expressed in this article are solely those of the authors and do not necessarily represent those of their affiliated organizations, or those of the publisher, editors, and reviewers. Any product that may be evaluated in this article, or claim that may be made by its manufacturer, is not guaranteed or endorsed by the publisher.

References

Allen, J. H. (2002). "Historical and recent solar activity and geomagnetic storms affecting spacecraft operations," in *Proceedings of the government* Microcircuit and applications conference (Monterey, CA: GOMAC'02).

Baker, D. N., Belian, R. D., Higbie, P. R., Klebesadel, R. W., and Blake, J. B. (1987). Deep dielectric charging effects due to high-energy electrons in Earth's outer magnetosphere. *J. Electrost.* 20 (1), 3–19. doi:10.1016/0304-3886(87)90082-9

Baker, D. N., Erickson, P. J., Fennell, J. F., Foster, J. C., Jaynes, A. N., and Verronen, P. T. (2018). Space weather effects in the Earth's radiation belts. *Space Sci. Rev.* 214 (1), 17–60. doi:10.1007/s11214-017-0452-7

Baker, D. N., Higbie, P. R., Belian, R. D., and Hones, E. W., Jr (1979). Do Jovian electrons influence the terrestrial outer radiation zone? *Geophys. Res. Lett.* 6 (6), 531–534. doi:10.1029/gl006i006p00531

Baker, D. N., Jaynes, A. N., Kanekal, S. G., Foster, J. C., Erickson, P. J., Fennell, J. F., et al. (2016). Highly relativistic radiation belt electron acceleration, transport, and loss: Large solar storm events of March and June 2015. *JGR. Space Phys.* 121 (7), 6647–6660. doi:10.1002/2016ja022502

Baker, D. N., Kanekal, S. G., and Blake, J. B. (2004). Characterizing the Earth's outer Van Allen zone using a radiation belt content index. *Space weather.* 2 (2). doi:10.1029/2003sw000026

Baker, D. N., Kanekal, S. G., Horne, R. B., Meredith, N. P., and Glauert, S. A. (2007). Low-altitude measurements of 2–6 MeV electron trapping lifetimes at 1.5≤ L≤ 2.5. *Geophys. Res. Lett.* 34 (20), L20110. doi:10.1029/2007gl031007

Benacquista, R., Boscher, D., Rochel, S., and Maget, V. (2018). Variations of the electron fluxes in the terrestrial radiation belts due to the impact of corotating interaction regions and interplanetary coronal mass ejections. *J. Geophys. Res. Space Phys.* 123 (2), 1191–1199. doi:10.1002/2017ja024796

Blake, J. B., Baker, D. N., Turner, N., Ogilvie, K. W., and Lepping, R. P. (1997). Correlation of changes in the outer-zone relativistic-electron population with upstream solar wind and magnetic field measurements. *Geophys. Res. Lett.* 24 (8), 927–929. doi:10.1029/97gl00859

Borovsky, J. E., and Birn, J. (2014). The solar wind electric field does not control the dayside reconnection rate. *J. Geophys. Res. Space Phys.* 119 (2), 751–760. doi:10.1002/2013ja019193

Borovsky, J. E., and Denton, M. H. (2010). Magnetic field at geosynchronous orbit during high-speed stream-driven storms: Connections to the solar wind, the plasma sheet, and the outer electron radiation belt. *J. Geophys. Res.* 115 (A8). doi:10.1029/2009ja015116

Borovsky, J. E., and Funsten, H. O. (2003). MHD turbulence in the Earth's plasma sheet: Dynamics, dissipation, and driving. *J. Geophys. Res.* 108 (A7), 1284. doi:10.1029/2002ja009625

Bortnik, J., Thorne, R. M., O'Brien, T. P., Green, J. C., Strangeway, R. J., Shprits, Y. Y., et al. (2006). Observation of two distinct, rapid loss mechanisms during the 20 November 2003 radiation belt dropout event. *J. Geophys. Res.* 111 (A12), A12216. doi:10.1029/2006ja011802

Boynton, R. J., Mourenas, D., and Balikhin, M. A. (2016). Electron flux dropouts at Geostationary Earth Orbit: Occurrences, magnitudes, and main driving factors. *J. Geophys. Res. Space Phys.* 121 (9), 8448–8461. doi:10.1002/2016ja022916

Boynton, R. J., Mourenas, D., and Balikhin, M. A. (2017). Electron flux dropouts at L~ 4.2 from global positioning system satellites: Occurrences, magnitudes, and main driving factors. *J. Geophys. Res. Space Phys.* 122 (11), 11–428. doi:10.1002/2017ja024523

Clilverd, M. A., Rodger, C. J., Andersson, M. E., Seppala, A., and Verronen, P. T. (2016). "Linkages between the radiation belts, polar atmosphere and climate: Electron precipitation through wave particle interactions," in *Waves particles and storms in geospace* (Oxford: Oxford University Press), 354–376.

Elkington, S. R., Hudson, M. K., and Chan, A. A. (2003). Resonant acceleration and diffusion of outer zone electrons in an asymmetric geomagnetic field. *J. Geophys. Res.* 108 (A3), 1116. doi:10.1029/2001ja009202

Friedel, R. H. W., Reeves, G. D., and Obara, T. (2002). Relativistic electron dynamics in the inner magnetosphere—a review. *J. Atmos. Solar-Terrestrial Phys.* 64 (2), 265–282. doi:10.1016/s1364-6826(01)00088-8

Gao, X., Li, W., Bortnik, J., Thorne, R. M., Lu, Q., Ma, Q., et al. (2015). The effect of different solar wind parameters upon significant relativistic electron flux dropouts in the magnetosphere. *JGR. Space Phys.* 120 (6), 4324–4337. doi:10.1002/2015ja021182

Gopalswamy, N., Yashiro, S., Michalek, G., Xie, H., Mäkelä, P., Vourlidas, A., et al. (2010). A catalog of halo coronal mass ejections from SOHO. *Sun Geosph.* 5 (1), 7–16.

Gopalswamy, N., Yashiro, S., Xie, H., Akiyama, S., and Mäkelä, P. (2015). Properties and geoeffectiveness of magnetic clouds during solar cycles 23 and 24. *JGR. Space Phys.* 120 (11), 9221–9245. doi:10.1002/2015ja021446

Green, J. C., Onsager, T. G., O'Brien, T. P., and Baker, D. N. (2004). Testing loss mechanisms capable of rapidly depleting relativistic electron flux in the Earth's outer radiation belt. *J. Geophys. Res.* 109 (A12), A12211. doi:10.1029/2004ja010579

Herrera, D., Maget, V. F., and Sicard Piet, A. (2016). Characterizing magnetopause shadowing effects in the outer electron radiation belt during geomagnetic storms. *JGR. Space Phys.* 121 (10), 9517–9530. doi:10.1002/2016ja022825

Hietala, H., Kilpua, E. K. J., Turner, D. L., and Angelopoulos, V. (2014). Depleting effects of ICME-driven sheath regions on the outer electron radiation belt. *Geophys. Res. Lett.* 41 (7), 2258–2265. doi:10.1002/2014gl059551

Horne, R. B., Thorne, R. M., Glauert, S. A., Albert, J. M., Meredith, N. P., and Anderson, R. R. (2005). Timescale for radiation belt electron acceleration by whistler mode chorus waves. *J. Geophys. Res.* 110 (A3), A03225. doi:10.1029/2004ja010811

Iles, R. H. A., Fazakerley, A. N., Johnstone, A. D., Meredith, N. P., and Bühler, P. (2002). The relativistic electron response in the outer radiation belt during magnetic storms. *Ann. Geophys.* 20, 957–965. doi:10.5194/angeo-20-957-2002

Kilpua, E. K. J., Balogh, A., Von Steiger, R., and Liu, Y. D. (2017b). Geoeffective properties of solar transients and stream interaction regions. *Space Sci. Rev.* 212 (3), 1271–1314. doi:10.1007/s11214-017-0411-3

Kilpua, E. K. J., Hietala, H., Turner, D. L., Koskinen, H. E. J., Pulkkinen, T. I., Rodriguez, J. V., et al. (2015). Unraveling the drivers of the storm time radiation belt response. *Geophys. Res. Lett.* 42 (9), 3076–3084. doi:10.1002/2015gl063542

Kilpua, E., Koskinen, H. E., and Pulkkinen, T. I. (2017a). Coronal mass ejections and their sheath regions in interplanetary space. *Living Rev. Sol. Phys.* 14 (1), 5–83. doi:10.1007/s41116-017-0009-6

Kim, H. J., and Chan, A. A. (1997). Fully adiabatic changes in storm time relativistic electron fluxes. *J. Geophys. Res.* 102 (A10), 22107–22116. doi:10.1029/97ja01814

Kim, K. C., Lee, D. Y., Kim, H. J., Lee, E. S., and Choi, C. R. (2010). Numerical estimates of drift loss and Dst effect for outer radiation belt relativistic electrons with arbitrary pitch angle. *J. Geophys. Res.* 115 (A3). doi:10.1029/2009ja014523

Koskinen, H. E., and Kilpua, E. K. (2022). *Physics of Earth's radiation belts: Theory and observations*. Springer Nature, 272.

Li, X., Baker, D. N., Temerin, M., Cayton, T. E., Reeves, E. G. D., Christensen, R. A., et al. (1997). Multisatellite observations of the outer zone electron variation during the November 3–4, 1993, magnetic storm. *J. Geophys. Res.* 102 (A7), 14123–14140. doi:10.1029/97ja01101

Li, X., Temerin, M., Baker, D. N., Reeves, G. D., and Larson, D. (2001). Quantitative prediction of radiation belt electrons at geostationary orbit based on solar wind measurements. *Geophys. Res. Lett.* 28 (9), 1887–1890. doi:10.1029/2000gl012681

Lyons, L. R., and Thorne, R. M. (1973). Equilibrium structure of radiation belt electrons. *J. Geophys. Res.* 78 (13), 2142–2149. doi:10.1029/ja078i013p02142

McIlwain, C. E. (1966). Ring current effects on trapped particles. *J. Geophys. Res.* 71 (15), 3623–3628. doi:10.1029/jz071i015p03623

Meredith, N. P., Cain, M., Horne, R. B., Thorne, R. M., Summers, D., and Anderson, R. R. (2003). Evidence for chorus-driven electron acceleration to relativistic energies from a survey of geomagnetically disturbed periods. *J. Geophys. Res.* 108 (A6), 1248. doi:10.1029/2002ja009764

Meredith, N. P., Horne, R. B., Lam, M. M., Denton, M. H., Borovsky, J. E., and Green, J. C. (2011). Energetic electron precipitation during high-speed solar wind stream driven storms. *J. Geophys. Res.* 116 (A5). doi:10.1029/2010ja016293

Millan, R. M., and Thorne, R. (2007). Review of radiation belt relativistic electron losses. *J. Atmos. Solar-Terrestrial Phys.* 69 (3), 362–377. doi:10.1016/j.jastp.2006.06.019

Miyoshi, Y., and Kataoka, R. (2005). Ring current ions and radiation belt electrons during geomagnetic storms driven by coronal mass ejections and corotating interaction regions. *Geophys. Res. Lett.* 32 (21), L21105. doi:10.1029/2005gl024590

Myllys, M., Kilpua, E. K. J., Lavraud, B., and Pulkkinen, T. I. (2016). Solar wind-magnetosphere coupling efficiency during ejecta and sheath-driven geomagnetic storms. *J. Geophys. Res. Space Phys.* 121 (5), 4378–4396. doi:10.1002/2016ja022407

Ni, B., Xiang, Z., Gu, X., Shprits, Y. Y., Zhou, C., Zhao, Z., et al. (2016). Dynamic responses of the Earth's radiation belts during periods of solar wind dynamic pressure pulse based on normalized superposed epoch analysis. *J. Geophys. Res. Space Phys.* 121 (9), 8523–8536. doi:10.1002/2016ja023067

Onsager, T. G., Rostoker, G., Kim, H. J., Reeves, G. D., Obara, T., Singer, H. J., et al. (2002). Radiation belt electron flux dropouts: Local time, radial, and particle-energy dependence. *J. Geophys. Res.* 107 (A11), 138221. doi:10.1029/2001ja000187

Palmroth, M., Partamies, N., Polvi, J., Pulkkinen, T. I., McComas, D. J., Barnes, R. J., et al. (2007). Solar wind–magnetosphere coupling efficiency for solar wind pressure impulses. *Geophys. Res. Lett.* 34 (11), L11101. doi:10.1029/2006gl029059

Paulikas, G. A., and Blake, J. B. (1979). Effects of the solar wind on magnetospheric dynamics: Energetic electrons at the synchronous orbit. *Quantitative Model. Magnetos. Process. Geophys. Monogr. Ser* 21, 180–202.

Pham, K. H., Tu, W., and Xiang, Z. (2017). Quantifying the precipitation loss of radiation belt electrons during a rapid dropout event. *JGR. Space Phys.* 122 (10), 10–287. doi:10.1002/2017ja024519

Pinto, V. A., Kim, H. J., Lyons, L. R., and Bortnik, J. (2018). Interplanetary parameters leading to relativistic electron enhancement and persistent depletion events at geosynchronous orbit and potential for prediction. *JGR. Space Phys.* 123 (2), 1134–1145. doi:10.1002/2017ja024902

Reeves, G. D., McAdams, K. L., Friedel, R. H. W., and O'brien, T. P. (2003). Acceleration and loss of relativistic electrons during geomagnetic storms. *Geophys. Res. Lett.* 30 (10). doi:10.1029/2002gl016513

Reeves, G. D., Spence, H. E., Henderson, M. G., Morley, S. K., Friedel, R. H. W., Funsten, H. O., et al. (2013). Electron acceleration in the heart of the Van Allen radiation belts. *Science* 341 (6149), 991–994. doi:10.1126/science.1237743

Richardson, I. G., and Cane, H. V. (2010). Near-Earth interplanetary coronal mass ejections during solar cycle 23 (1996–2009): Catalog and summary of properties. *Sol. Phys.* 264 (1), 189–237. doi:10.1007/s11207-010-9568-6

Selvakumaran, R., Veenadhari, B., Akiyama, S., Pandya, M., Gopalswamy, N., Yashiro, S., et al. (2016). On the reduced geoeffectiveness of solar cycle 24: A moderate storm perspective. *J. Geophys. Res. Space Phys.* 121 (9), 8188–8202. doi:10.1002/2016ja022885

Shprits, Y. Y., Drozdov, A. Y., Spasojevic, M., Kellerman, A. C., Usanova, M. E., Engebretson, M. J., et al. (2016). Wave-induced loss of ultra-relativistic electrons in the Van Allen radiation belts. *Nat. Commun.* 7 (1), 12883–12887. doi:10.1038/ncomms12883

Shprits, Y. Y., Thorne, R. M., Friedel, R., Reeves, G. D., Fennell, J., Baker, D. N., et al. (2006). Outward radial diffusion driven by losses at magnetopause. *J. Geophys. Res.* 111 (A11), A11214. doi:10.1029/2006ja011657

Shue, J. H., Chao, J. K., Fu, H. C., Russell, C. T., Song, P., Khurana, K. K., et al. (1997). A new functional form to study the solar wind control of the magnetopause size and shape. *J. Geophys. Res.* 102 (A5), 9497–9511. doi:10.1029/97ja00196

Souza, V. M., Lopez, R. E., Jauer, P. R., Sibeck, D. G., Pham, K., Da Silva, L. A., et al. (2017). Acceleration of radiation belt electrons and the role of the average interplanetary magnetic field Bz component in high-speed streams. *J. Geophys. Res. Space Phys.* 122 (10), 10–084.

Staples, F. A., Rae, I. J., Forsyth, C., Smith, A. R. A., Murphy, K. R., Raymer, K. M., et al. (2020). Do statistical models capture the dynamics of the magnetopause during sudden magnetospheric compressions? *J. Geophys. Res. Space Phys.* 125 (4), e2019JA027289. doi:10.1029/2019ja027289

Summers, D., Thorne, R. M., and Xiao, F. (1998). Relativistic theory of wave-particle resonant diffusion with application to electron acceleration in the magnetosphere. *J. Geophys. Res.* 103 (A9), 20487–20500. doi:10.1029/98ja01740

Thorne, R. M., and Kennel, C. (1971). Relativistic electron precipitation during magnetic storm main phase. *J. Geophys. Res.* 76 (19), 4446–4453. doi:10.1029/ja076i019p04446

Tsurutani, B. T., Hajra, R., Tanimori, T., Takada, A., Remya, B., Mannucci, A. J., et al. (2016). Heliospheric plasma sheet (HPS) impingement onto the magnetosphere as a cause of relativistic electron dropouts (REDs) via coherent EMIC wave scattering with possible consequences for climate change mechanisms. *J. Geophys. Res. Space Phys.* 121 (10), 10–130. doi:10.1002/2016ja022499

Turner, D. L., Angelopoulos, V., Li, W., Bortnik, J., Ni, B., Ma, Q., et al. (2014). Competing source and loss mechanisms due to wave-particle interactions in Earth's outer radiation belt during the 30 September to 3 October 2012 geomagnetic storm. *JGR. Space Phys.* 119 (3), 1960–1979. doi:10.1002/2014ja019770

Turner, D. L., Kilpua, E. K. J., Hietala, H., Claudepierre, S. G., O'Brien, T. P., Fennell, J. F., et al. (2019). The response of Earth's electron radiation belts to geomagnetic storms: Statistics from the Van Allen Probes era including effects from different storm drivers. *JGR. Space Phys.* 124 (2), 1013–1034. doi:10.1029/2018ja026066

Turner, D. L., Shprits, Y., Hartinger, M., and Angelopoulos, V. (2012). Explaining sudden losses of outer radiation belt electrons during geomagnetic storms. *Nat. Phys.* 8 (3), 208–212. doi:10.1038/nphys2185

Xiang, Z., Tu, W., Li, X., Ni, B., Morley, S. K., and Baker, D. N. (2017). Understanding the mechanisms of radiation belt dropouts observed by Van Allen Probes. *JGR. Space Phys.* 122 (10), 9858–9879. doi:10.1002/2017ja024487

Yermolaev, Y. I., Nikolaeva, N. S., Lodkina, I. G., and Yermolaev, M. Y. (2010). Specific interplanetary conditions for CIR-Sheath-and ICME-induced geomagnetic storms obtained by double superposed epoch analysis. *Ann. Geophys.* 28, 2177–2186. doi:10.5194/angeo-28-2177-2010

Yuan, C., and Zong, Q. (2013). Relativistic electron fluxes dropout in the outer radiation belt under different solar wind conditions. *J. Geophys. Res. Space Phys.* 118 (12), 7545–7556. doi:10.1002/2013ja019066

Yue, C., and Zong, Q. (2011). Solar wind parameters and geomagnetic indices for four different interplanetary shock/ICME structures. *J. Geophys. Res.* 116 (A12). doi:10.1029/2011ja017013

Zhang, X. J., Li, W., Thorne, R. M., Angelopoulos, V., Ma, Q., Li, J., et al. (2016). Physical mechanism causing rapid changes in ultrarelativistic electron pitch angle distributions right after a shock arrival: Evaluation of an electron dropout event. *JGR. Space Phys.* 121 (9), 8300–8316. doi:10.1002/2016ja022517